



**HAL**  
open science

## Sorption strains and their consequences for capillary condensation in nanoconfinement

Gerrit Günther, Martin Schoen

► **To cite this version:**

Gerrit Günther, Martin Schoen. Sorption strains and their consequences for capillary condensation in nanoconfinement. *Molecular Simulation*, 2009, 35 (01-02), pp.138-150. 10.1080/08927020802412370 . hal-00515057

**HAL Id: hal-00515057**

**<https://hal.science/hal-00515057>**

Submitted on 4 Sep 2010

**HAL** is a multi-disciplinary open access archive for the deposit and dissemination of scientific research documents, whether they are published or not. The documents may come from teaching and research institutions in France or abroad, or from public or private research centers.

L'archive ouverte pluridisciplinaire **HAL**, est destinée au dépôt et à la diffusion de documents scientifiques de niveau recherche, publiés ou non, émanant des établissements d'enseignement et de recherche français ou étrangers, des laboratoires publics ou privés.

## Sorption strains and their consequences for capillary condensation in nanoconfinement

Journal:	<i>Molecular Simulation</i> / <i>Journal of Experimental Nanoscience</i>
Manuscript ID:	GMOS-2008-0108.R2
Journal:	Molecular Simulation
Date Submitted by the Author:	11-Aug-2008
Complete List of Authors:	Günther, Gerrit; Technische Universität Berlin, Stranski-Lab. f. Physikalische und Theoretische Chemie Schoen, Martin; Technische Universität Berlin, Stranski-Lab. f. Physikalische und Theoretische Chemie
Keywords:	Sorption strain, capillary condensation, nanoconfined fluids, Monte Carlo simulation

SCHOLARONE™  
Manuscripts

# Sorption strains and their consequence for capillary condensation in nanoconfinement

Gerrit Günther\* and Martin Schoen†

*Stranski-Laboratorium für Physikalische und Theoretische Chemie, Sekr. C 7,  
Fakultät für Mathematik und Naturwissenschaften, Technische Universität Berlin,  
Straße des 17. Juni 135, D-10623 Berlin, Germany*

(Dated: August 5, 2008)

## Abstract

We employ Monte Carlo simulations in a semi-grand canonical ensemble to investigate the impact of pore deformation on capillary condensation in nanoconfined fluids. The fluid is composed of “simple” spherically symmetric molecules of the Lennard-Jones type. These molecules are confined to a slit-pore where the pore walls consist of a single layer of atoms distributed according to the (100) plane of the face-centered cubic lattice. The atoms are bound to their equilibrium lattice sites by harmonic potentials such that they can depart to some extent from these sites on account of their thermal energy and the interaction with the fluid molecules. Under experimentally realistic conditions our results show that upon filling with fluid the effective average pore size first increases, then drops sharply at capillary condensation. The pore eventually expands again when the density of the confined liquid-like phase is further enhanced. Compared with the ideal case of perfectly rigid substrates deformability of the pore causes capillary condensation to shift to higher bulk pressures, that is the liquid-like phases are destabilized relative to confined gas-like phases.

PACS numbers: 02.70.Uu,64.70.fm,64.75.Jk,68.35.Rh

---

\*Electronic address: [gerrit.guenther@fluids.tu-berlin.de](mailto:gerrit.guenther@fluids.tu-berlin.de)

†Electronic address: [martin.schoen@fluids.tu-berlin.de](mailto:martin.schoen@fluids.tu-berlin.de)

## I. INTRODUCTION

If a fluid is exposed to an external field its phase behavior and materials properties will depend on the specific characteristics of the field. In the context of confined fluids the solid matrix of a mesoporous material has frequently been treated as such an external field representing the walls of tiny pores of nanometer dimensions [1–3]. When adsorbed into these pores their small size (i.e., the strength of the external field) causes a markedly different phase behavior, structure, and materials properties of the adsorbate. For example, **if the fluid-substrate attraction is sufficiently strong** condensation of the adsorbate occurs under thermodynamic conditions such that a corresponding bulk fluid is still an undersaturated gas. This phenomenon known as “capillary condensation” is in principle predicted by the celebrated Kelvin equation [4] and has received quite a bit of experimental interest [5–10]. However, these early studies were basically concerned with disordered porous media such as, for example, controlled pore glasses where the pores vary in shape and form an interconnected network. In the meantime it has become feasible to synthesize other mesoporous materials that differ from the ones studied in these earlier works in that they consist of more regular arrays of individual, disconnected, more or less cylindrical pores [11–13]. These new materials enable studies of nanoconfined fluids under more controlled conditions.

The experimental advances have also spurred a wealth of theoretical investigations of confined fluids from which a detailed molecular picture of capillary condensation emerged [1–3]. One of the most intriguing theoretical findings in more recent times concerns the prediction of novel phases in fluids confined between complex chemically decorated or geometrically sculptured substrates [14, 15]. Here the confined fluids’ structure is imposed by the substrates through a template effect. Thus, these new confined thermodynamic phases have obviously no counterpart in any bulk system which makes them particularly fascinating.

However, regardless of the specific nature of the model system studied theoretically, the confining substrates are conventionally treated as an inhomogeneous, anisotropic, but otherwise static external field. From this perspective characteristic features of a confined fluid come about by superimposing the external field onto the intermolecular interactions between fluid molecules. In other words, no matter what changes occur in a confined fluid’s thermodynamic state or mechanical properties the solid substrates do not “respond” or adjust themselves to any of these changes.

1  
2  
3  
4  
5  
6  
7  
8  
9  
10  
11  
12  
13  
14  
15  
16  
17  
18  
19  
20  
21  
22  
23  
24  
25  
26  
27  
28  
29  
30  
31  
32  
33  
34  
35  
36  
37  
38  
39  
40  
41  
42  
43  
44  
45  
46  
47  
48  
49  
50  
51  
52  
53  
54  
55  
56  
57  
58  
59  
60

However, quite some time ago Diestler and Schoen showed that the mechanical properties and the structure of a confined fluid may be altered if the confining substrates are coupled thermally to the fluid phase [16]. The physical situation studied in Ref. 16 is relevant to experimental work by Namatsu *et al.* in which the authors show that thin silica plates separated by a distance of less than 200 nm may deform during the drying process after having been rinsed by water [17]. More recently, Kowalczyk *et al.* [18] and Ustinov and Do [19] considered sorption-induced deformation of porous matrices. In both works the pores may deform *homogeneously*, that is the width of the entire pore may change upon increasing sorption. However, these earlier papers [18, 19] do not explore the relation between capillary condensation and pore deformation.

Moreover, it was recently demonstrated experimentally that SBA-15 pores may be deformed upon capillary condensation. Using *in-situ* synchrotron X-ray diffraction (SAXD) and parallel measurements of an adsorption isotherm Zickler *et al.* demonstrated that a discontinuous phase transition in a confined fluid may alter the lattice constant characterizing the (regular) mesoporous matrix [20]. In Ref. 20 the correlation between the associated sorption strains and capillary condensation is established by comparing form, location, and intensity of the Bragg peaks determined in the scattering experiments with the steep variation of the adsorption isotherm at capillary condensation.

Sorption strains of the sort reported in Ref. 20 have also been observed earlier experimentally [21–23] and are discussed in terms of either continuum elasticity [21] or phenomenological thermodynamics [22]. It is also well-known from solid-solid phase transitions that elastic strains may cause a shift of the phase boundaries [24]. However, to date a microscopic analysis of the relationship between sorption strains and phase transitions in nanoconfined is still lacking.

In the present work we therefore intend to employ Monte Carlo simulations to address the following questions in conjunction with capillary condensation in a nanopore with *locally* deformable pore walls (*cf.*, Refs. 18 and 19):

1. How are sorption strains related to the thermodynamic state of the confined fluid?
2. Do sorption strains have an impact on capillary condensation?
3. What is the relation between sorption strains and the structure of the confined fluid?

To address these points we organized the manuscript as follows. In Sec. II we introduce our model system and describe its thermodynamic and statistical physical analysis in Secs. III A and III B, respectively. A key quantity that we wish to compute is the grand-potential density  $\omega$  of the confined fluid. We obtain  $\omega$  via thermodynamic perturbation theory as we explain in Sec. III C. In Sec. IV A we analyze the relation between substrate deformation and capillary condensation whereas Sec. IV B is devoted to associated structural changes in the confined fluid. The paper concludes with a summary of our main findings in Sec. V.

## II. MODEL SYSTEM

### A. The model fluid

In this work we consider a pure fluid consisting of  $N$  spherically-symmetric molecules interacting with each other in a pairwise additive fashion. The fluid-fluid configurational energy can then be cast as

$$U_{\text{ff}}(\mathbf{R}) = \frac{1}{2} \sum_{i=1}^N \sum_{j=1 \neq i}^N u(r_{ij}) \quad (2.1)$$

where  $r_{ij} = |\mathbf{r}_i - \mathbf{r}_j|$  is the distance between molecules  $i$  and  $j$  located at  $\mathbf{r}_i$  and  $\mathbf{r}_j$ , respectively,  $\mathbf{R} \equiv (\mathbf{r}_1, \mathbf{r}_2, \dots, \mathbf{r}_N)$  represents the configuration of fluid molecules,

$$u(r) = \begin{cases} u_{\text{sh}}(r), & r \leq r_c \\ 0, & r > r_c \end{cases} \quad (2.2)$$

and

$$u_{\text{sh}}(r) = u_{\text{LJ}}(r) - u_{\text{LJ}}(r_c) + \left. \frac{du_{\text{LJ}}(r)}{dr} \right|_{r=r_c} (r - r_c) \quad (2.3)$$

is a so-called shifted-force potential. Unlike the full Lennard-Jones (LJ) potential

$$u_{\text{LJ}}(r) = 4\varepsilon \left[ \left( \frac{\sigma}{r} \right)^{12} - \left( \frac{\sigma}{r} \right)^6 \right] \quad (2.4)$$

$u_{\text{sh}}(r)$  vanishes continuously together with its first derivative (i.e., the intermolecular force) at the radius  $r_c$  of a cutoff sphere centered on  $\mathbf{r}_i$ . Throughout this work we use  $r_c = 3.5\sigma$ . Because of its definition  $u_{\text{sh}}(r)$  is explicitly short-range [unlike  $u_{\text{LJ}}(r)$ ] which is advantageous in the Monte Carlo (GCEMC) simulations on which this work is based [3, 25]. In Eq. (2.4),  $\sigma$  is the “diameter” of a fluid molecule and  $\varepsilon$  determines the strength of intermolecular interactions in the usual manner.

## B. Thermally coupled substrates

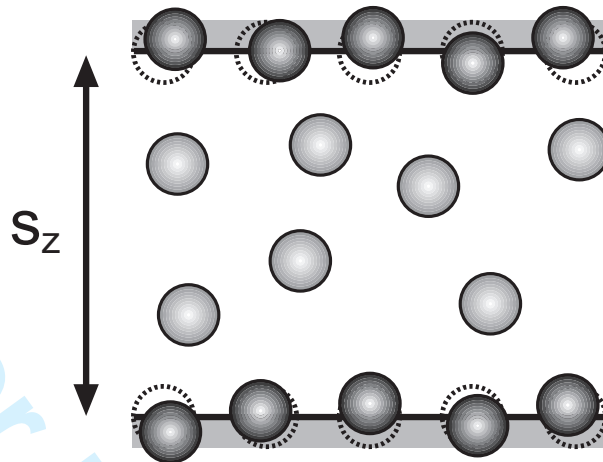


FIG. 1: Two-dimensional schematic representation of the model system consisting of spherical fluid molecules (light grey) confined between two planar solid substrates separated by a distance  $s_z$  along the  $z$ -axis of the Cartesian coordinate system. In the reference system the substrates are structureless as indicated by the black vertical line and the area shaded in grey above and below this line. In the system of interest the homogeneous substrates are replaced by discrete wall atoms (dark grey) where the equilibrium fcc (100) positions are represented by dashed circles.

Fluid molecules are confined by two planar solid substrates (see Fig. 1). For reasons that will become clear in Sec. III we need to consider a reference system, in which fluid molecules are confined between two structureless, planar substrates. In the system of ultimate interest the walls are thermally coupled to the confined fluid such that the walls can respond to whatever change in the thermodynamic state of the confined fluid may occur. In this latter case the substrates are atomically structured and thermally corrugated as indicated by the sketch in Fig. 1.

In both cases there is a fluid-solid contribution to the total configurational energy. For the reference system this contribution may be expressed as

$$U_{\text{fs}}^{\text{ref}} = \sum_{k=1}^2 \sum_{i=1}^N \varphi^{[k]}(z_i) \quad (2.5)$$

where the fluid-solid interaction potential is given by

$$\varphi^{[k]}(z) = 2\pi\varepsilon\rho_s\sigma^2 \left[ \frac{2}{5} \left( \frac{\sigma}{z \pm s_z/2} \right)^{10} - \left( \frac{\sigma}{z \pm s_z/2} \right)^4 \right] \quad (2.6)$$

In Eq. (2.6),  $k = 1 \leftrightarrow +$  and  $k = 2 \leftrightarrow -$ , respectively and we assume the solid substrates to be located at  $z = \pm s_z/2$ . Equation (2.6) is derived on the basis of the assumption that the substrate is composed of a single layer of solid atoms. **These atoms are positioned according to the (100) structure of the face-centered cubic (fcc) lattice such that the nearest-neighbor distance between the atoms corresponds to the minimum of  $u(r)$ . This implies a lattice constant  $\ell/\sigma = \sqrt[3]{4}$  such that the areal density  $\rho_s\sigma^2 = 2/\ell^2$ .** The solid atoms have been “smeared” over the plane while the position of a fluid molecule is fixed at a point  $\mathbf{r}_i$  [3]. Moreover, we take the parameters  $\sigma$  and  $\varepsilon$  to be the same for fluid molecules and wall atoms during the course of a simulation.

To realize walls that can respond to the confined fluid we introduce our model of interest. **Again the substrates consist of individual solid atoms initially distributed according to the (100) plane of the fcc lattice at the areal density given above.** The planes are **initially** in registry, that is a specific atom in the upper substrate is exactly opposite its counterpart in the lower one and vice versa. This way the confined fluid can only be subjected to compressional strains (by changing, for example,  $s_z$  through external agents) but not to any shear deformation. Taking fluid molecules and substrate atoms to be identical (i.e., taking  $\sigma$  and  $\varepsilon$  to be the same for both species) we replace Eq. (2.5) by

$$U_{\text{fs}}(\mathbf{R}, \mathbf{R}_s) = \zeta \sum_{k=1}^2 \sum_{i=1}^N \sum_{j=1}^{N_s} u\left(\left|\mathbf{r}_i - \mathbf{r}_j^{[k]}\right|\right) \quad (2.7)$$

where  $N_s = 2n^2$  is the total number of substrate atoms located in one wall and  $n$  is an integer specifying the number of unit cells of the fcc (100) plane. In Eq. (2.7),  $\mathbf{R}_s = \left(\mathbf{r}_1^{[1]}, \dots, \mathbf{r}_{N_s}^{[1]}, \mathbf{r}_1^{[2]}, \dots, \mathbf{r}_{N_s}^{[2]}\right)$  represents the configuration of substrate atoms. The potential  $u$  in Eq. (2.7) is given in Eq. (2.2). **The dimensionless parameter  $\zeta$  in Eq. (2.7) is introduced to vary the strength of the fluid-substrate interaction [see Eqs. (2.2) – (2.4), Eq. (2.7), and Sec. IV B]. If not stated otherwise results in Sec. IV are obtained for the case  $\zeta = 1.0$  referring to equally strong fluid-fluid and fluid-substrate interactions. In any event, the distribution of the solid atoms and the rigidity of the substrates is such that fluid molecules cannot penetrate into the confining substrates as we have checked for all the simulations reported here.**

In addition to  $U_{fs}$  we include interactions between the substrate atoms themselves. The corresponding solid-solid energy is composed of two contributions and may be expressed as

$$U_{ss} = \sum_{k=1}^2 \left[ \frac{1}{2} \sum_{i=1}^{N_s} \sum_{j=1 \neq i}^{N_s} u \left( \left| \mathbf{r}_i^{[k]} - \mathbf{r}_j^{[k]} \right| \right) + \kappa \sum_{i=1}^{N_s} \left| \mathbf{r}_i^{[k]} - \mathbf{r}_{i0}^{[k]} \right|^2 \right] \quad (2.8)$$

where  $u$  is again given by Eq. (2.2). On account of their interaction with both fluid molecules and other substrate atoms each of the latter is free to depart from its equilibrium position ( $\mathbf{r}_{i0}^{[k]}$ ) in the fcc (100) plane. In other words, substrate atoms are coupled thermally to the confined fluid and may move because of their kinetic energy. The first term on the right side of Eq. (2.8) is necessary because substrate atoms must not approach each other arbitrarily (and therefore unrealistically) close. To prevent the substrates from “melting” we bind each one of them to its equilibrium lattice site by introducing a harmonic potential [see second term in brackets in Eq. (2.8)] where  $\kappa > 0$  determines the binding strength (i.e., the “stiffness” of a harmonic spring). In other words,  $\kappa$  is a measure of rigidity of the substrates. Hence, in the system of interest the total configurational energy may be expressed [see Eqs. (2.1), (2.7), and (2.8)] as

$$U(\mathbf{R}, \mathbf{R}_s; \kappa) = U_{ff}(\mathbf{R}) + U_{fs}(\mathbf{R}, \mathbf{R}_s) + U_{ss}(\mathbf{R}_s; \kappa) \quad (2.9)$$

and depends on  $\mathbf{R}$ ,  $\mathbf{R}_s$ , and  $\kappa$  as a parameter.

### III. THEORETICAL CONSIDERATIONS

#### A. Thermodynamics

To mimic a situation frequently encountered in sorption experiments we treat the confined fluid as a semi-open system within the framework of phenomenological thermodynamics. This perception is motivated by the fact that in parallel sorption experiments the fluid confined to some mesoporous matrix is assumed to be in thermodynamic equilibrium with a (quasi-infinite) bulk reservoir with which it may exchange fluid matter and heat. Under these conditions and for a quantitative discussion of phase behavior of the confined fluid the semi-grand potential  $\Omega$  turns out to be the relevant thermodynamic potential. Following

the treatment of Ref. 3 the exact differential of  $\Omega$  may be cast as

$$\begin{aligned} d\Omega(T, \mu, N_s, \boldsymbol{\sigma}) = & -\mathcal{S}dT - Nd\mu + 2\mu_s dN_s \\ & + V_0 \text{Tr}(\boldsymbol{\tau}d\boldsymbol{\sigma}) \end{aligned} \quad (3.1)$$

where  $T$  denotes temperature,  $\mathcal{S}$  entropy,  $\mu$  and  $\mu_s$  are the chemical potentials of fluid molecules and substrate atoms, respectively, and  $V_0 = s_{x0}s_{y0}s_{z0}$  is the volume of a finite rectangular lamella of the confined fluid in an (yet to be specified) unstrained reference state where  $s_{\alpha 0}$  is the side length of the lamella in the (Cartesian)  $\alpha$ -direction; the remainder of the infinitely large confined fluid constitutes the surroundings of the lamella in the usual thermodynamic sense.

In Eq. (3.1) the mechanical work contribution is expressed in terms of the trace  $\text{Tr}$  of a product of stress  $\boldsymbol{\tau}$  and conjugate (infinitesimal) strain tensors  $d\boldsymbol{\sigma}$  [3]. As demonstrated in Ref. 3 these quantities can be represented by symmetric  $3 \times 3$  matrices. Employing Cartesian coordinates and in the absence of shear strains we have

$$\boldsymbol{\tau} = \frac{1}{2} \begin{pmatrix} 2\tau_{xx} & \tau_{xy} & \tau_{xz} \\ \tau_{xy} & 2\tau_{yy} & \tau_{yz} \\ \tau_{xz} & \tau_{yz} & 2\tau_{zz} \end{pmatrix} \quad (3.2a)$$

$$\begin{aligned} \boldsymbol{\sigma} &= \begin{pmatrix} \sigma_{xx} & 0 & 0 \\ 0 & \sigma_{yy} & 0 \\ 0 & 0 & \sigma_{zz} \end{pmatrix} \\ &= \begin{pmatrix} \tilde{s}_x/s_{x0} - 1 & 0 & 0 \\ 0 & \tilde{s}_y/s_{y0} - 1 & 0 \\ 0 & 0 & \tilde{s}_z/s_{z0} - 1 \end{pmatrix} \end{aligned} \quad (3.2b)$$

where  $\tilde{s}_\alpha$  denotes the side lengths of a rectangular lamella of the fluid in a strained state.

Equations (3.1)–(3.2b) apply to the system of interest, namely a slit-pore with thermally corrugated walls as the most general case. These expressions become somewhat simpler for the reference system. Because in this latter case the walls lack any distinct atomic structure the fluid is isotropic in the  $x$ – $y$  plane perpendicular to the confining substrates. We may exploit this isotropy and define

$$\tau_{\parallel} \equiv \tau_{xx} = \tau_{yy} \quad (3.3a)$$

$$\frac{\sigma_{\parallel}}{2} \equiv \sigma_{xx} = \sigma_{yy} \quad (3.3b)$$

Moreover, we may reexpress  $V_0$  as

$$V_0 = s_{x0}s_{y0}s_{z0} = A_0s_{z0} \quad (3.4)$$

where  $A_0$  is the area of the  $z$ -directed face of the lamella in the unstrained reference state. Introducing  $A = \sigma_{\parallel}A_0$  as the  $z$ -directed area of the lamella in a strained state it is straightforward to verify from Eqs. (3.2)–(3.4) that

$$\begin{aligned} d\Omega(T, \mu, N_s, A, s_z) &= -SdT - Nd\mu + 2\mu_s dN_s \\ &\quad + \tau_{\parallel}s_{z0}dA + \tau_{zz}A_0ds_z \end{aligned} \quad (3.5)$$

It is then also clear that the confined fluid is *homogeneous* across each of the  $x$ – $y$  planes stacked along the  $z$ -direction. Therefore,  $\Omega$  in Eq. (3.5) turns out to be a homogeneous function of degree 1 in its extensive (natural) variable  $A$ . We may therefore employ Euler's theorem (see Appendix A.3 of Ref. 3) and introduce the semi-grand potential density of the reference system via

$$\omega^{\text{ref}} \equiv \frac{\Omega^{\text{ref}}}{As_{z0}} = \frac{\Omega^{\text{ref}}}{V} = \tau_{\parallel}^{\text{ref}}, \quad T, \mu, N_s, s_z = \text{const} \quad (3.6)$$

A similar expression does not obtain for the system of interest because the discrete (atomic) structure of the substrates destroys homogeneity and isotropy of the confined fluid in the  $x$ – $y$  plane. However, regardless of the validity of Eq. (3.6) the (exact) thermodynamic relations

$$\left( \frac{\partial \omega}{\partial \mu} \right)_{\{\cdot\}} = -\rho < 0 \quad (3.7a)$$

$$\left( \frac{\partial^2 \omega}{\partial \mu^2} \right)_{\{\cdot\}} = -\rho^2 \kappa_T < 0 \quad (3.7b)$$

hold where  $\rho \equiv \langle N \rangle / V$  is the mean (number) density of the fluid,  $\kappa_T$  is its isothermal compressibility, and  $\{\cdot\}$  is shorthand notation to indicate that the differentiation is to be performed with  $T$ ,  $N_s$ , and  $\sigma$  being held fixed. Because of equations (3.7a) and (3.7b) we conclude that curves  $\omega(\mu)$  are monotonously decaying and concave.

Thus, under favorable thermodynamic conditions one anticipates phase coexistence at intersections  $\mu_x^{\alpha\beta}$  at which

$$\omega^{\alpha}(\mu_x^{\alpha\beta}) = \omega^{\beta}(\mu_x^{\alpha\beta}) \quad (3.8)$$

for a pair of phases  $\alpha$  and  $\beta$ . Suppose  $\rho^{\alpha} < \rho^{\beta}$  it follows that phase  $\alpha$  is thermodynamically stable for  $\mu < \mu_x^{\alpha\beta}$  whereas phase  $\beta$  is stable if the inequality  $\mu > \mu_x^{\alpha\beta}$  holds.

## B. Statistical thermodynamics

The connection with a microscopic level of description is established by statistical thermodynamics. To that end

$$\Omega(T, \mu, N_s, \boldsymbol{\sigma}) = -k_B T \ln \Xi(T, \mu, N_s, \boldsymbol{\sigma}) \quad (3.9)$$

is the key expression where  $k_B$  is Boltzmann's constant and

$$\Xi(T, \mu, N_s, \boldsymbol{\sigma}) = \sum_{N=0}^{\infty} \exp(\beta \mu N) \mathcal{Q}(T, N, N_s, \boldsymbol{\sigma}) \quad (3.10)$$

is the semi-grand canonical partition function where  $\beta \equiv 1/k_B T$  [26].

In the classical limit, with which we are exclusively concerned in this work, the canonical-ensemble partition function may be cast as

$$\mathcal{Q} = \frac{\mathcal{Z}}{\Lambda^{3(N+2N_s)} N!} \quad (3.11)$$

where

$$\Lambda = \frac{h}{\sqrt{2\pi m k_B T}} \quad (3.12)$$

is the thermal de Broglie wavelength. The specific form of Eq. (3.11) results from an integration over momentum subspace formed by the  $N$  fluid molecules and  $2N_s$  substrate atoms each of which possess three translational degrees of freedom. Substrate atoms, which are bound to their equilibrium lattice sites [see Eq. (2.8)], are distinguishable such that only the factor  $1/N!$  arises for the (indistinguishable) fluid molecules in the denominator of Eq. (3.11).

For our system of interest the configuration integral in Eq. (3.11) is given by

$$\mathcal{Z}(T, N, N_s, \boldsymbol{\sigma}) = \int d\mathbf{R} \int d\mathbf{R}_s \exp[-\beta U(\mathbf{R}, \mathbf{R}_s; \kappa)] \quad (3.13)$$

where the dependence on the (compressional) strains  $\boldsymbol{\sigma}$  is buried in the limits of integration with respect to fluid-particle coordinates. The integration over substrate-atom configurations reflects the thermal coupling between the substrate and the confined fluid. In other words, for finite  $\kappa$  the substrates cannot be treated as an external field but are part of the system in the same spirit in which the configuration of a disordered porous matrix enters the statistical physical analysis of quenched-annealed models of complex mesoporous materials (see, for example, Chap. 7.2 of Ref. 3). From Eqs. (2.9), (3.1), and (3.9)–(3.13) all microscopic expressions for thermomechanical properties of the system of interest can be derived [16].

However, in this work we are concerned with the phase behavior of the confined fluid. As we will explain shortly (see Sec. III C) this requires a computation of the stress  $\tau_{\parallel}$  acting in directions perpendicular to the substrate normal in the *reference* system. According to Sec. II B the substrates in the reference system are both structureless [see Eqs. (2.5) and (2.6)] and rigid. Because of these features we may replace  $\mathcal{Z}(T, N, N_s, \boldsymbol{\sigma})$  by the simpler expression

$$\mathcal{Z}^{\text{ref}}(T, N, A, s_z) = \int d\mathbf{R} \exp[-\beta(U_{\text{ff}} + U_{\text{fs}}^{\text{ref}})] \quad (3.14)$$

In Eq. (3.14),  $U_{\text{fs}}^{\text{ref}}$  depends only on the  $z$ -coordinates of the fluid molecules. Thus,  $U_{\text{fs}}^{\text{ref}}$  may be interpreted as the potential energy due to a static, inhomogeneous, external field acting on a configuration of fluid molecules in the  $z$ -direction. From Eqs. (3.5), (3.9), (3.11), and (3.14) it is then a simple matter to verify that

$$\begin{aligned} \tau_{\parallel}^{\text{ref}} &= \frac{1}{s_{z0}} \left( \frac{\partial \Omega^{\text{ref}}}{\partial A} \right)_{\{\cdot\}} = -\frac{k_B T}{s_{z0}} \left( \frac{\partial \ln \Xi^{\text{ref}}}{\partial A} \right)_{\{\cdot\}} \\ &= -\frac{\langle N \rangle k_B T}{V} + \frac{1}{4V} \left\langle \sum_{i=1}^N \sum_{j=1 \neq i}^N u'(r_{ij}) r_{ij} \right. \\ &\quad \left. \times [(\hat{\mathbf{r}}_{ij} \cdot \hat{\mathbf{e}}_x)^2 + (\hat{\mathbf{r}}_{ij} \cdot \hat{\mathbf{e}}_y)^2] \right\rangle \end{aligned} \quad (3.15)$$

where  $\mathbf{r} = r\hat{\mathbf{r}}$ , and  $\hat{\mathbf{e}}_{\alpha}$  is a unit vector along the  $\alpha$ -axis of the (Cartesian) coordinate system. In Eq. (3.15) angular brackets denote ensemble averages in the grand canonical ensemble such that together Eqs. (3.6) and (3.15) provide a “mechanical” molecular route to the grand-potential density.

### C. Perturbation theory

Unfortunately, such a “mechanical” expression for  $\omega$  does not exist for the system of interest (see Sec. III A and Ref. 27). To compute  $\omega$  for our system of interest despite this deficiency in symmetry we employ thermodynamic perturbation theory as suggested by Zwanzig back in 1954 [28] (see also Refs. 3 and 26) and write

$$\begin{aligned} U(\lambda) &= U_{\text{ff}} + (1 - \lambda) U_{\text{fs}}^{\text{ref}} + \lambda(U_{\text{fs}} + U_{\text{ss}}) \\ &\equiv U_{\text{ff}} + U_{\text{fs}}^{\text{ref}} + \lambda\Phi \end{aligned} \quad (3.16)$$

for the total configurational energy where  $\lambda \in [0, 1]$  is a dimensionless parameter serving as a (continuous) “switch” between the reference system ( $\lambda = 0$ ) and the system of interest

( $\lambda = 1$ ). The function  $\Phi$  is introduced in Eq. (3.16) merely for notational convenience.

Through Eqs. (3.9)–(3.11), (3.13), and (3.16) it is then evident that the (semi-) grand potential formally becomes a function of the coupling parameter  $\lambda$ . Thus, we may differentiate  $\Omega(\lambda)$  with respect to the coupling parameter and obtain

$$\begin{aligned} \frac{d\Omega(\lambda)}{d\lambda} &= \frac{1}{\Xi(\lambda)} \sum_{N=0}^{\infty} \frac{\exp(\beta\mu N)}{\Lambda^{3(N+2N_s)} N!} \\ &\quad \times \int d\mathbf{R} \int d\mathbf{R}_s \Phi(\mathbf{R}, \mathbf{R}_s; \kappa) \exp[-\beta U(\lambda)] \\ &= \langle \Phi(\mathbf{R}, \mathbf{R}_s; \kappa) \rangle_{\lambda} \end{aligned} \quad (3.17)$$

In Eq. (3.17) the angular brackets denote an average in the (semi-) grand canonical ensemble in which the distribution of microstates is governed by  $U(\lambda)$  for a particular value of the coupling parameter  $\lambda$ . We may formally integrate this last expression which gives

$$\begin{aligned} \omega(\lambda) &= \omega(0) + \frac{1}{V} \int_0^{\lambda} d\lambda' \langle \Phi(\mathbf{R}, \mathbf{R}_s; \kappa) \rangle_{\lambda'} \\ &= \tau_{\parallel}^{\text{ref}} + \frac{1}{V} \int_0^{\lambda} d\lambda' \langle \Phi(\mathbf{R}, \mathbf{R}_s; \kappa) \rangle_{\lambda'} \end{aligned} \quad (3.18)$$

The expression on the second line of Eq. (3.18) follows because  $\lambda = 0$  corresponds to the reference system [see Eq. (3.16)] where Eq. (3.6) holds.

#### IV. RESULTS

Henceforth, all quantities are expressed in suitable dimensionless (i.e., “reduced”) units. For example, energies are given in units of  $\varepsilon$ , temperature in units of  $\varepsilon/k_B$ , and length in units of  $\sigma$ . Other quantities like stress, density, or the binding parameter are expressed in terms of combinations of these “basic” units such as  $\varepsilon/\sigma^3$ ,  $\sigma^3$ , or  $\varepsilon/\sigma^2$ , respectively. **Unless otherwise stated all the simulations are carried out at a sufficiently subcritical temperature  $T = 1.0$ .**

##### A. Phase behavior and substrate “softness”

Equation (3.18) permits numerical access to the grand-potential density of the system of interest  $\omega(\lambda = 1)$ . Operationally speaking we need to compute  $\tau_{\parallel}^{\text{ref}}$  via Eq. (3.15) and

1  
2  
3  
4  
5  
6  
7  
8  
9  
10  
11  
12  
13  
14  
15  
16  
17  
18  
19  
20  
21  
22  
23  
24  
25  
26  
27  
28  
29  
30  
31  
32  
33  
34  
35  
36  
37  
38  
39  
40  
41  
42  
43  
44  
45  
46  
47  
48  
49  
50  
51  
52  
53  
54  
55  
56  
57  
58  
59  
60

$\langle \Phi(\mathbf{R}, \mathbf{R}_s; \kappa) \rangle_\lambda$  in a sequence of (typically 10–20) individual Monte Carlo simulations for discrete values  $0 \leq \lambda \leq 1$ . The integral in Eq. (3.18) is then evaluated numerically by means of a standard quadrature algorithm [29].

To illustrate this procedure we plot in Fig. 2,  $\omega(\lambda)$  for  $\kappa = 10^4$  and 30. A binding strength of  $\kappa = 10^4$  is large enough to prevent substrate atoms from departing appreciably from their equilibrium lattice sites during the course of the simulation. In other words,  $\kappa = 10^4$  corresponds to the limiting case of a perfectly rigid substrate for all practical purposes. This is because even vanishingly minute deviations of the actual position of any substrate atom from its equilibrium lattice site are associated with a substantial potential-energy penalty [see Eq. (2.8)].

As can be seen from respective plots in Figs. 2(a) and 2(b) data sets coincide for  $\lambda = 0$  corresponding to the reference system as they must. At the lower value  $\kappa = 30$  the substrate may be deformed on account of the interaction with neighboring substrate atoms, the coupling to the confined fluid, and the thermal energy of each substrate atom. However, plots in Fig. 2 shows that regardless of  $\kappa$ ,  $\omega(\lambda)$  is a monotonically decreasing function of the coupling parameter where the magnitude of the grand-potential is the smaller the more rigid the substrate is. The deviation between both data sets increases slightly with increasing  $\lambda$ .

The monotonicity of  $\omega(\lambda)$  is an important prerequisite for the perturbational approach described in Sec. III C. A monotonic variation of  $\omega$  with  $\lambda$  implies that the confined fluid does not undergo a first-order phase transition during the course of the transformation.

The perturbational procedure described in Sec. III C and illustrated by plots in Fig. 2 now permits us to compute  $\omega(\mu)$  along an isotherm that is subcritical with respect to the critical point of the fluid in confinement. To this end we need to choose two initial values of the chemical potential  $\mu_{\text{in}}$  corresponding to the one-phase region of confined gas- and liquid-like phases. These values of the chemical potential are not known *a priori* so that some trial and error is required at this point.

We may then use  $\mu_{\text{in}}$  in the reference system and compute  $\omega(\mu_{\text{in}})$  in the system of interest via Eq. (3.18). Once this value of the grand potential is known we may use Eq. (3.7a) in its integrated form

$$\omega(\mu) = \omega(\mu_{\text{in}}) - \int_{\mu_{\text{in}}}^{\mu} d\mu' \rho(\mu'), \quad T = \text{const} \quad (4.1)$$

for different values of  $\mu$ . The mean (number) density  $\rho(\mu)$  appearing in the integrand in

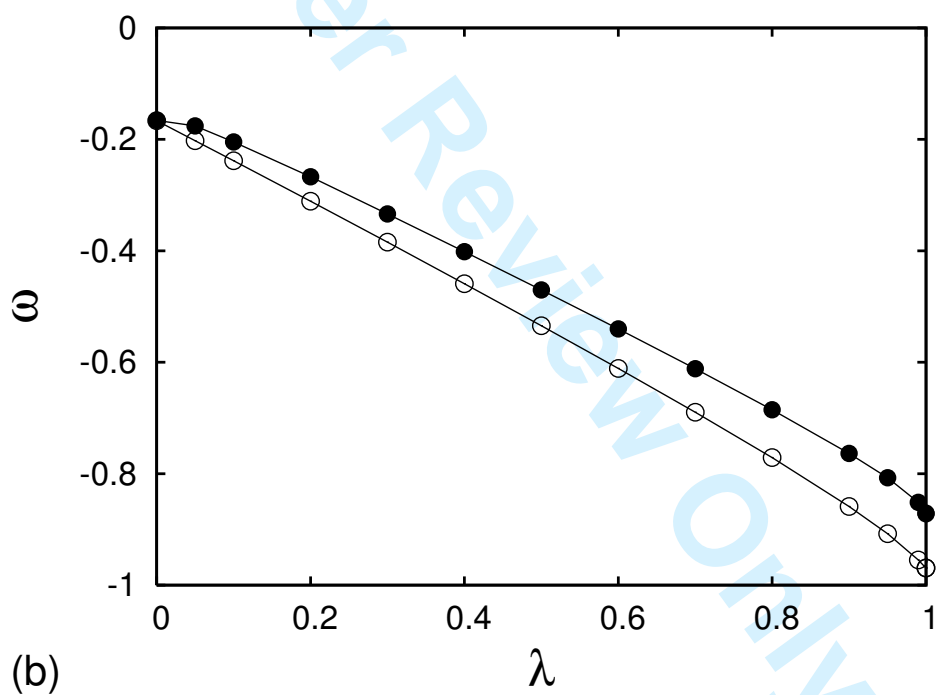
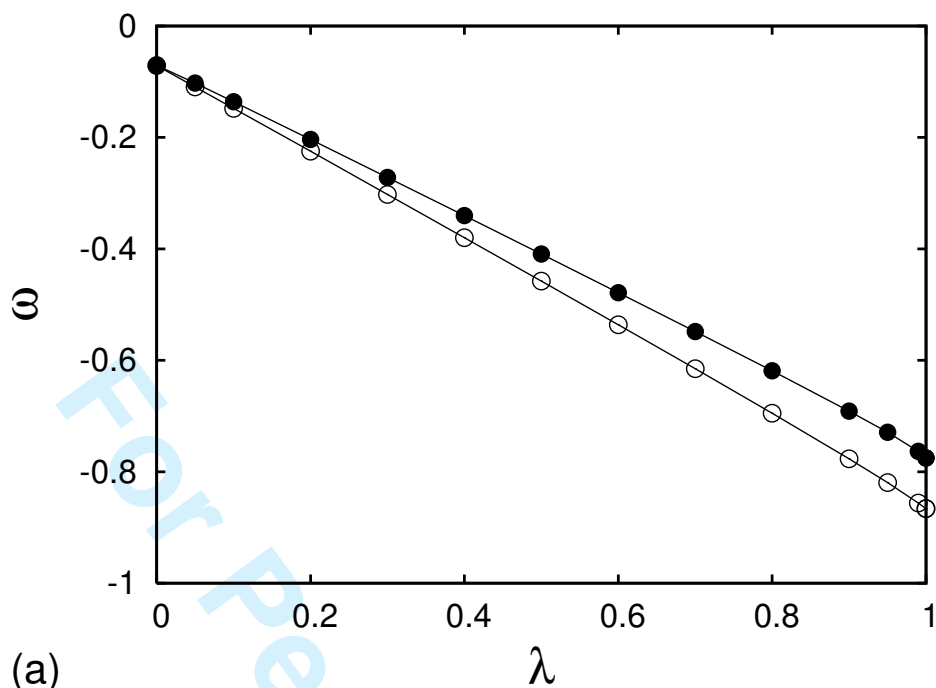


FIG. 2: Plot of  $\omega$  as a function of the coupling parameter  $\lambda$  [see Eq. (3.18)] for  $\kappa = 10^4$  ( $\circ$ ) and  $\kappa = 30$  ( $\bullet$ ). (a) gas-like phases,  $\mu = -11.6$ , (b) liquid-like phases,  $\mu = -11.3$ .

Eq. (4.1) is computed as an ensemble average in semi-grand canonical ensemble Monte Carlo (SGCMC) simulations.

To analyze confinement effects and in particular the impact of substrate “softness” on capillary condensation it is necessary to determine first the location of the gas-liquid phase transition in the bulk. For a given subcritical temperature this can be done in a straightforward fashion by computing the grand-potential density in SGCMC simulations from

$$\omega = -P = -\frac{\langle N \rangle k_B T}{V} + \frac{1}{6V} \left\langle \sum_{i=1}^N \sum_{j=1 \neq i}^N u'(r_{ij}) r_{ij} \right\rangle \quad (4.2)$$

This expression follows by noting that in a homogeneous and isotropic bulk phase the mechanical-work term in Eq. (3.1) can be simplified to  $V_0 \text{Tr}(\boldsymbol{\tau} d\boldsymbol{\sigma}) = -PdV$  where  $P$  is the (scalar) bulk pressure [3]. By manipulations similar to those leading to Eq. (3.15) one may then derive the molecular expression for the bulk pressure on the far right side of Eq. (4.2) (see, for example, Appendix E.3.3 of Ref. 3).

As expected from the discussion in Sec. III A a plot of  $\omega(\mu)$  consists of two branches. According to Eq. (3.7a) the one with the smaller (magnitude of the) slope (at smaller values of the chemical potential) along a subcritical isotherm  $T = 1.0$  corresponds to gas whereas the one with the larger (magnitude of the) slope pertains to liquid phases. Both branches intersect at the chemical potential of gas-liquid coexistence  $\mu_x^{\text{gl}} \simeq -11.16$ . At this point the slope of  $\omega(\mu)$  changes discontinuously because the densities of gas  $\rho_x^g \simeq 0.059$  and liquid phases  $\rho_x^l \simeq 0.634$  are different at coexistence [see Eq. (3.7a)].

If one confines the fluid to a slit pore with a substrate separation  $s_z = 6.8$  one expects a shift of gas-liquid phase coexistence to smaller bulk pressures because of the additional fluid-substrate attraction. Indeed defining a reduced pressure  $P/P_0$  ( $P_0$  pressure of the saturated bulk gas at  $\mu_x^{\text{gl}} \simeq -11.16$  and  $T = 1.0$ ) the bulk phase transition occurs at  $P/P_0 = 1$  which is outside the range of (reduced) pressures plotted in Fig. 3(b). Therefore, the plot in Fig. 3(b) reveals such a shift to a reduced pressure  $P/P_0 \simeq 0.69$  as far as the (quasi-)rigid substrate at  $\kappa = 10^4$  is concerned.

If one now couples the substrate thermally to the confined fluid by reducing the binding strength to  $\kappa = 30$  the plots in Fig. 3(b) show the enhanced deformability of the substrate that causes a shift of the coexistence pressure to a larger value  $P/P_0 \simeq 0.72$ . In other words, a slightly larger bulk pressure (or chemical potential  $\mu$ ) is required to initiate capillary condensation in the slit-pore if the substrates respond to the phase change in the fluid

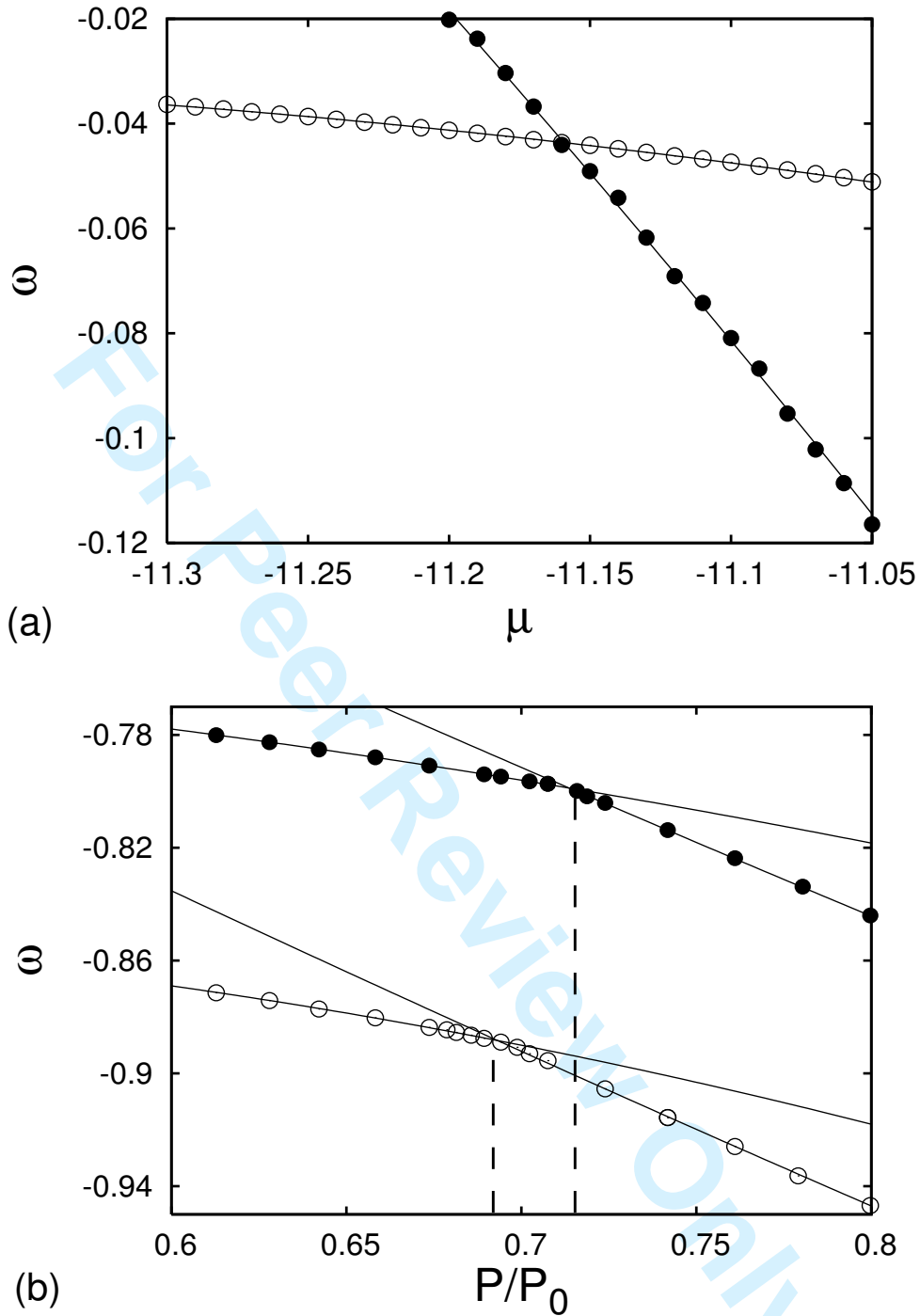


FIG. 3: (a) The grand-potential density  $\omega$  as a function of  $\mu$  in the bulk ( $T = 1.0$ ). (b) As (a) but for a fluid confined to a slit-pore ( $s_z = 6.8$ ) as a function of  $P/P_0$  in a corresponding bulk system where  $P_0 = 0.043$  is determined from the plot in part (a) of this figure; (○)  $\kappa = 10^4$ , (●)  $\kappa = 30$ . The vertical dashed line demarcates  $\mu_x^{gl}$  (see text).

material that they confine. Thus, a deformable substrate destabilizes confined liquid-like phases relative to the perfectly rigid substrate.

If the fluid is confined to a narrower slit-pore of  $s_z = 5.6$ , capillary condensation occurs at a lower pressure  $P/P_0 \simeq (\kappa = 10^4)$  and  $P/P_0 \simeq (\kappa = 30)$  in accord with one's physical intuition [see Fig. 4(a)]. A similar shift is observed if one maintains the pore width at  $s_z = 6.8$  but reduces the temperature to  $T = 0.8$  [see Fig. 4(b)]. However, in both cases it is noteworthy that  $\mu_x^{\text{gl}}$  is always larger for the deformable substrate compared with the (quasi-) rigid one.

## B. Structural aspects

At this point it seems worthwhile to address the associated structural changes both in the substrate and in the confined fluid that occur on account of capillary condensation. We begin by considering the local density

$$\rho^{\text{f,s}}(z) \equiv \frac{\langle N_{\text{f,s}}(z) \rangle}{A_0 \delta s_z} \quad (4.3)$$

where the sub- and superscripts “f” and “s” are used to refer to the local density of the confined fluid and to that of the substrate atoms, respectively. Thus,  $N_{\text{f,s}}(z)$  is the respective number of fluid molecules or substrate atoms located in a parallelepiped of dimensions  $s_{x0} \times s_{y0} \times \delta s_z$  centered on  $z$  where we take  $\delta s_z = 0.02$ .

A typical plot of the local densities for the (quasi-)rigid ( $\kappa = 10^4$ ) and a thermally coupled substrate ( $\kappa = 30$ ) are presented in Fig. 5 for the case  $s_z = 6.8$ . In the case of the (quasi-)rigid substrates

$$\rho^{\text{s}}(z) = \delta(z^{[1]} + s_z/2) + \delta(z^{[2]} - s_z/2) \quad (4.4)$$

where  $\delta$  denotes the Dirac  $\delta$ -function. As pointed out in Sec. III B at  $\kappa = 10^4$  the confining substrates may be perceived as an inhomogeneous, static external field imposed on the fluid molecules. As a consequence the fluid appears to be stratified, that is the centers of mass of fluid molecules arrange themselves preferentially in individual layers parallel with the substrate surfaces. Stratification of confined fluid phases is a well-known feature that has been noted many times in previous literature for various systems and confinement scenarios such as hard spheres between hard surfaces [30, 31], or soft spheres between atomically

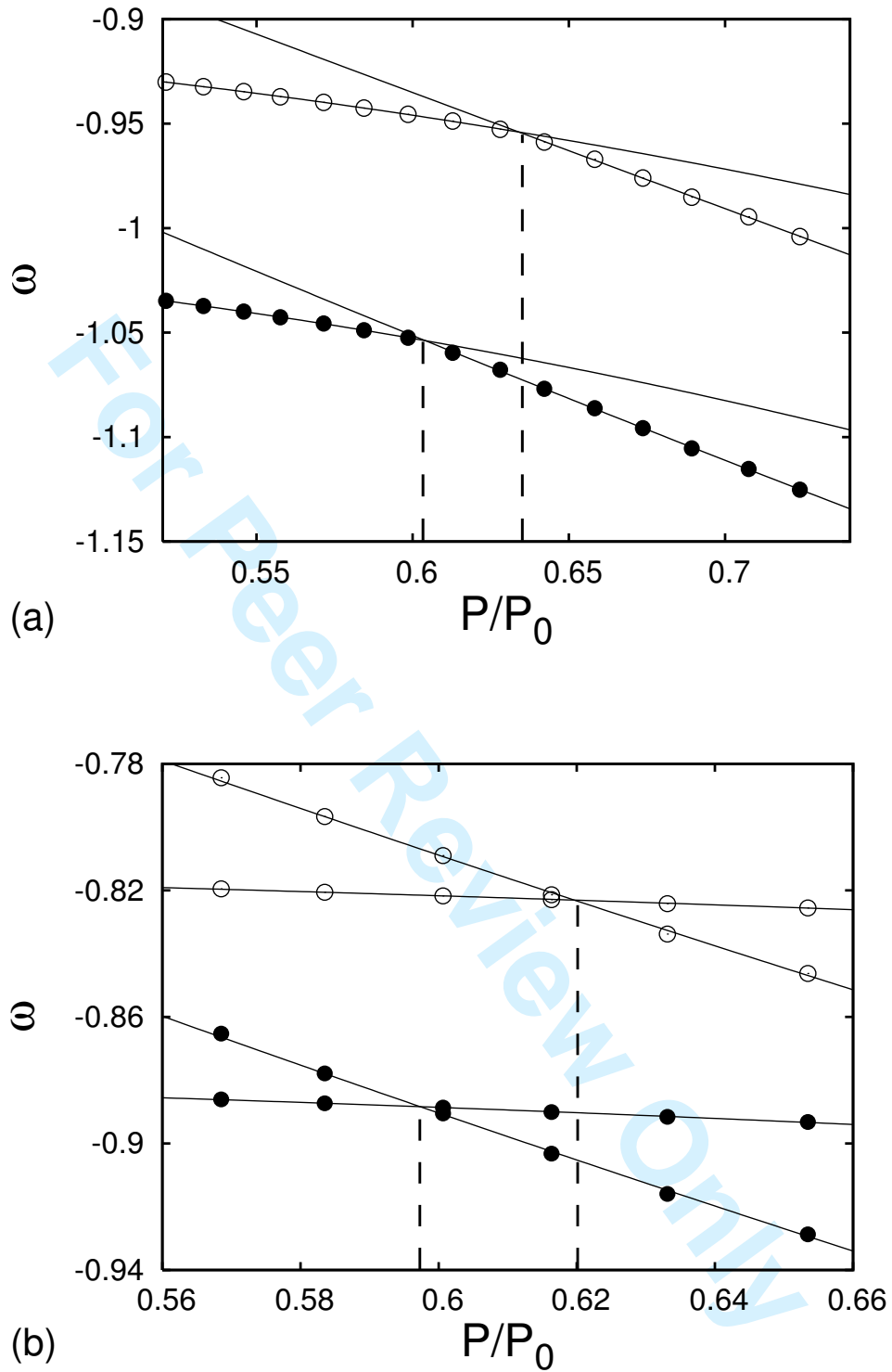


FIG. 4: As Fig. 3(b) but for  $s_z = 5.6$ ,  $T = 1.0$  (a) and  $s_z = 6.8$ ,  $T = 0.8$  (b), respectively.

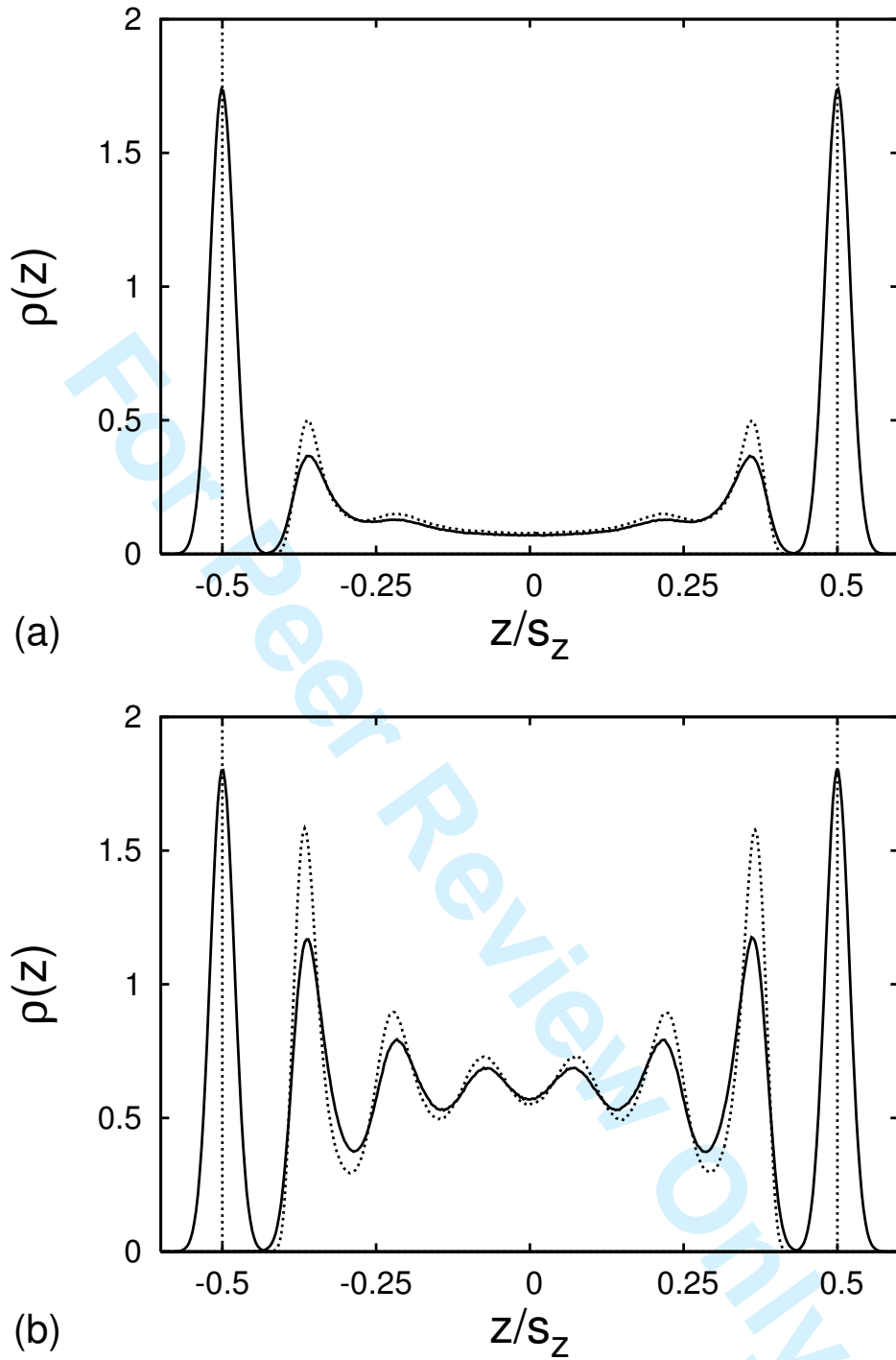


FIG. 5: Plots of  $\rho^s(z)$  and  $\rho^f(z)$  as functions of position  $z/s_z$  ( $s_z = 6.8$ ); quasi-rigid, atomically structured substrate, thermally coupled substrate at  $\kappa = 10^4$  ( $\cdots$ ) and  $\kappa = 30$  ( $—$ ). The portion of  $\rho(z)$  centered on  $|z|/s_z = 0.5$  refers to  $\rho^s(z)$  whereas the remainder of the curves corresponds to  $\rho^f(z)$ ; (a)  $\mu = -11.6$  ( $P/P_0 \simeq 0.58$ ), (b)  $\mu = -11.3$  ( $P/P_0 \simeq 0.84$ ).

smooth [32] or structured substrates [33, 34]. In addition, the substrates may be chemically patterned [15, 35] or nonplanar [36–38]. Even in more complex fluids consisting of non-spherical molecules stratification has been reported [39–42]. However, compared with fluids composed of spherically symmetric molecules stratification appears to be diminished in the former cases on account of internal degrees of freedom.

In the present case stratification diminishes as the substrate becomes increasingly deformable as one can see by comparing plots of  $\rho^f(z)$  for the (quasi-) rigid substrate ( $\kappa = 10^4$ ) with the corresponding data for the “softer” substrate at  $\kappa = 30$  [see Figs. 5(a) and 5(b)]. For this latter set of data maxima are generally lower and minima less shallow than for  $\kappa = 10^4$ . The effects are more pronounced in Fig. 5(b) than in Fig. 5(a) on account of the higher density of liquid-like confined fluids compared with gas-like states. However, stratification in general diminishes as the distance from both walls becomes larger because of the decreasing importance of fluid-substrate interactions. This effect is also confirmed by the plots in Fig. 5.

Moreover, an inspection of Fig. 5 also shows that  $\rho^s(z)$  for the thermally coupled substrate ( $\kappa = 30$ ) cannot be represented by a  $\delta$ -function but appears to be broadened because the substrate atoms possess thermal energy. For the time being, let us assume an ideal situation in which no fluid molecules are present between the substrates and we have switched off the coupling between neighboring substrate atoms by setting  $u\left(\left|\mathbf{r}_i^{[k]} - \mathbf{r}_j^{[k]}\right|\right) = 0$  [see Eq. (2.8)]. Because in this special case

$$U(\mathbf{R}_s) = \kappa \sum_{k=1}^2 \sum_{i=1}^{N_s} \left| \mathbf{r}_i^{[k]} \pm \frac{s_z}{2} \right|^2 \quad (4.5)$$

the probability of finding *any* substrate atom at a position  $z$  is given by

$$\begin{aligned} P(z) &= \frac{1}{2} \sqrt{\frac{\kappa}{\pi k_B T}} \left\{ \exp[-\beta \kappa (z - s_z/2)^2] \right. \\ &\quad \left. + \exp[-\beta \kappa (z + s_z/2)^2] \right\} \\ &\equiv P_-(z) + P_+(z) \end{aligned} \quad (4.6)$$

that is a distribution consisting of two Gaussians centered at  $z = \pm s_z/2$  provided that  $\beta \kappa$  is sufficiently large. Notice that in the limit  $\kappa \rightarrow \infty$ , Eq. (4.6) is consistent with Eq. (4.4) if we employ the definition of the Dirac  $\delta$ -function via Gaussian distributions (see, for example, Appendix B.6.1 in Ref. 3).

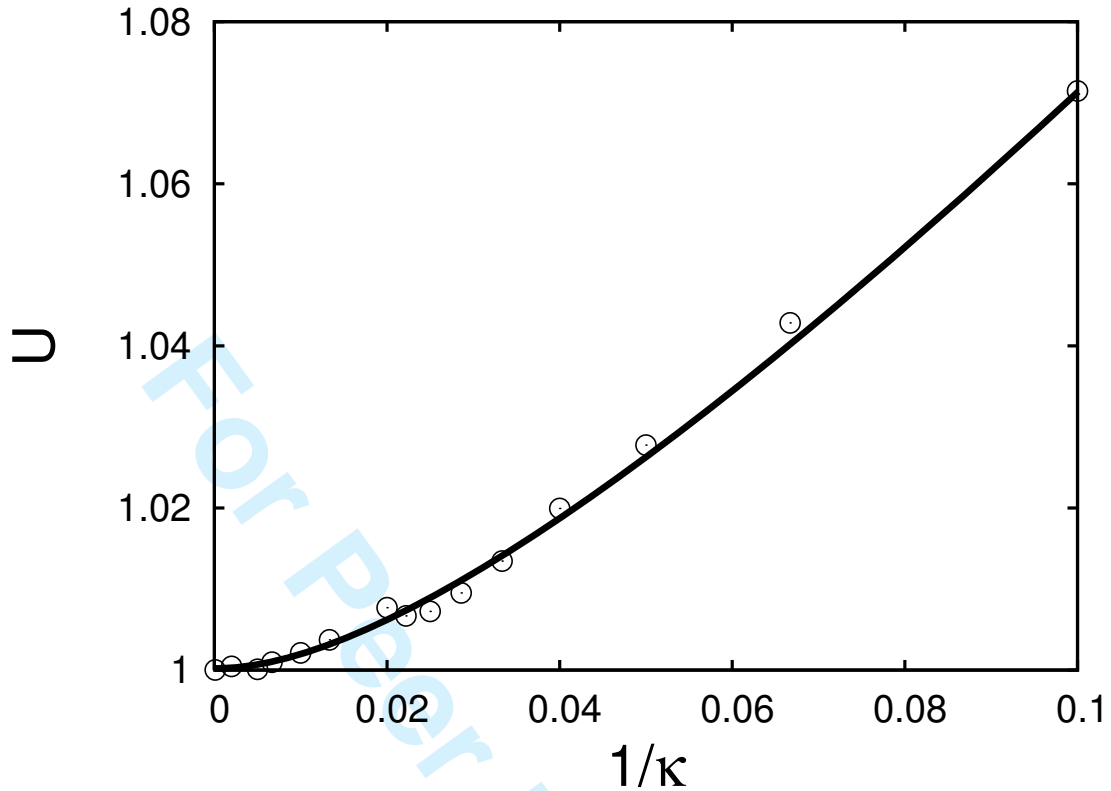


FIG. 6: The skewness parameter  $U$  as a function of inverse binding strength  $1/\kappa$ .

For the system of interest in which substrate atoms are coupled to one another and to a confined fluid of nonvanishing density one anticipates deviations from this “ideal” Gaussian form of the probability distributions. To quantify these deviations we focus on the central moments of the distributions  $P_{\pm}(z)$  defined via

$$\left\langle \left( z \pm \frac{s_z}{2} \right)^n \right\rangle \equiv \int_{-\infty}^{\infty} dz \left( z \pm \frac{s_z}{2} \right)^n P_{\pm}(z) \quad (4.7)$$

where  $P_{\pm}(z)$  is either given by  $P_+(z)$  or  $P_-(z)$  defined in Eq. (4.6). Equation (4.7) is particularly useful for two reasons. First, for even  $n$  one can verify by straightforward manipulations that

$$U \equiv \frac{3 \langle (z \pm s_z/2)^2 \rangle^2}{\langle (z \pm s_z/2)^4 \rangle} = 1 \quad (4.8)$$

if  $P_{\pm}(z)$  are Gaussian. In turn, any deviation of the previous expression from the (ideal) value of 1 indicates a certain skewness of the probability distribution. Second, if the distribution possesses such a skewness moments of odd order  $n$  do not necessarily vanish. In

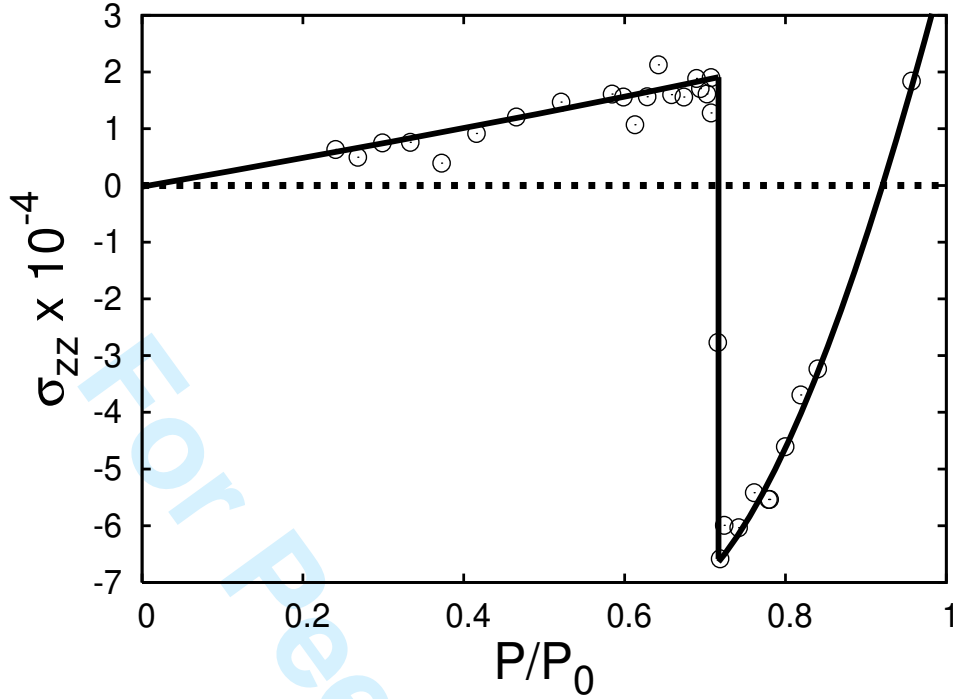


FIG. 7: The compressional stress  $\sigma_{zz}$  as a function of reduced bulk pressure  $P/P_0$  for a slit-pore of width  $s_z = 6.8$  and  $T = 1.0$ . (O)  $\kappa = 30$  where the solid line is used to guide the eye, ( $\cdots$ )  $\kappa = 10^4$ .

particular,

$$\langle z \rangle_{\pm} \equiv \int_{-\infty}^{\infty} dz z P_{\pm}(z) \quad (4.9)$$

such that an *effective* slit-pore width may be defined via

$$s_z^{\text{eff}} \equiv \langle z \rangle_{-} - \langle z \rangle_{+} \quad (4.10)$$

In the ideal case of Gaussian distributions  $P_{\pm}(z)$ ,  $s_z^{\text{eff}} = s_z$  because it is easy to verify from the previous expression that then  $\langle z \rangle_{\pm} = \mp s_z/2$ . Plots in Fig. 6 show that deviations from a Gaussian form of the density profile associated with the substrate atoms are minute but increase with decreasing “stiffness” (i.e., increasing  $1/\kappa$ ) with which substrate atoms are bound to their equilibrium lattice sites.

Let us now take the fluid confined between (quasi-) rigid walls ( $\kappa = 10^4$ ) as the unstrained reference state in the sense of the thermodynamic analysis presented in Sec. III A such that

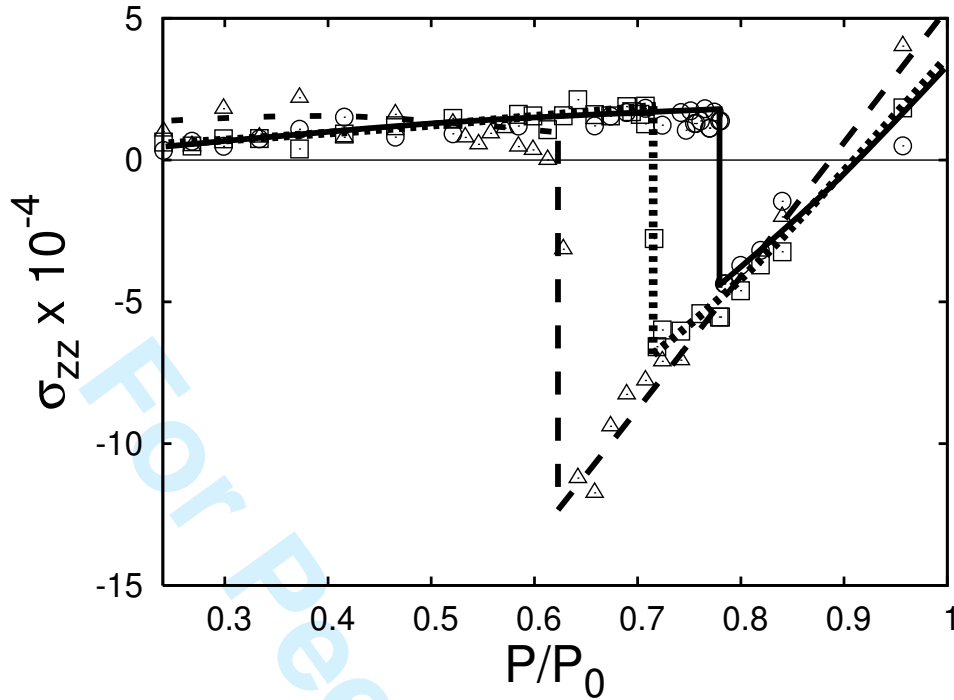


FIG. 8: As Fig. 7, but for  $s_z = 5.6$  ( $\Delta$ ),  $s_z = 6.8$  ( $\square$ ), and  $s_z = 8.0$  ( $\circ$ );  $T = 1.0$  and  $\kappa = 30$  for all data sets and lines are intended to guide the eye.

$s_{z0} = s_z$ . This permits us to define the compressional strain  $\sigma_{zz}$  [see Eq. (3.2b)] in the direction of the substrate normal as

$$\sigma_{zz} = \frac{s_z^{\text{eff}} - s_z}{s_z} \quad (4.11)$$

An inspection of the plot of  $\sigma_{zz}$  in Fig. 7 shows that the compressional strain increases at low pressures indicating that for a confined gas-like phase the slit-pore expands at first. Then, upon capillary condensation, it suddenly contracts but expands again as the pressure in the confined liquid-like phase is further raised. That the discontinuous change in  $\sigma_{zz}$  is, in fact, a signature of capillary condensation becomes evident upon comparison with the plot in Fig. 3(b) which indicates that capillary condensation arises at  $P/P_0 \simeq 0.72$ . The sequence of initial expansion, sudden contraction at capillary condensation, and subsequent expansion of the slit-pore is characteristic and qualitatively independent of both pore width (see Fig. 8) and temperature over the range of  $P/P_0$  studied. From the plots in Fig. 8 one notices that the value of  $P/P_0$  at capillary condensation increases with pore width  $s_z$  as

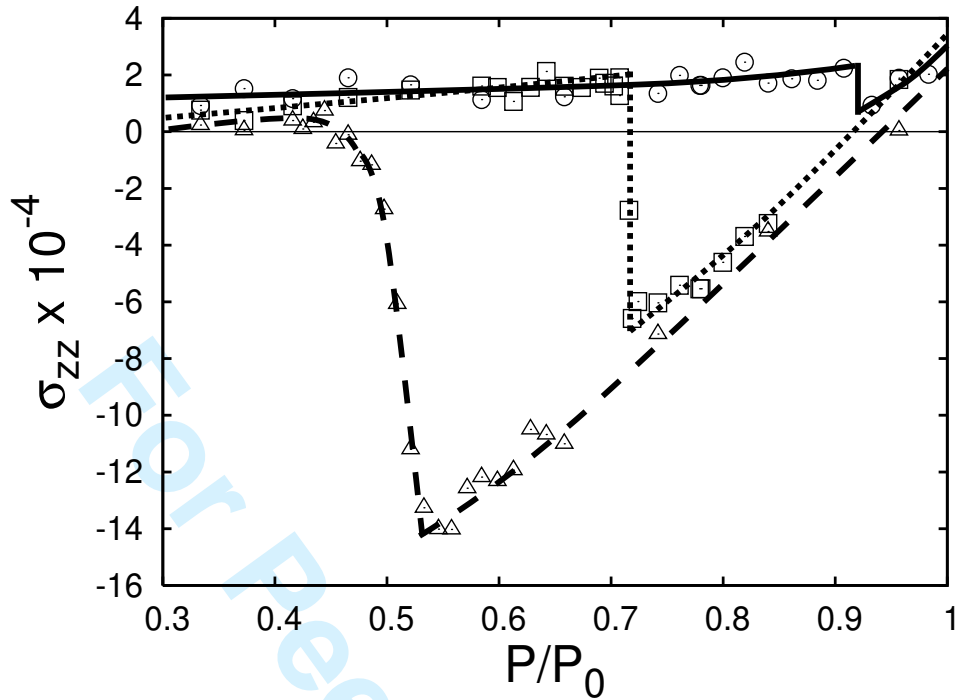


FIG. 9: As Fig. 7, but  $\zeta = 0.75$  ( $\Delta$ ),  $\zeta = 1.0$  ( $\square$ ), and  $\zeta = 1.5$  ( $\circ$ ) [see Eq. (2.7)];  $T = 1.0$ ,  $\kappa = 30$ , and  $s_z = 6.8$  for all data sets. Lines are intended to guide the eye.

one would expect. Likewise the magnitude of the discontinuous change in  $\sigma_{zz}$  at capillary condensation shrinks which is again in accord with one's physical intuition. Thus, both the variation of  $\sigma_{zz}$  with  $P$  and that of  $P/P_0$  at capillary condensation with  $\kappa$  are *generic* features associated with sorption strains. Moreover, the variation of  $\sigma_{zz}$  with  $P$  plotted in Fig. 7 is consistent with data obtained in recent SAXD experiments of **nonpolar fluids** confined to mesoporous silica [45].

However, qualitative changes in the compressional strain arise if one varies the strength of the fluid-substrate attraction as plots in Fig. 9 reveal. For example, for weak fluid-substrate interactions ( $\zeta = 0.75$ ) the plot of  $\sigma_{zz}$  increases weakly up to  $P/P_0 \simeq 0.9$  where capillary condensation sets in. The discontinuity in the sorption strain at capillary condensation is, on the other hand, more pronounced for equally strong fluid-fluid and fluid-substrate interactions as the plot of  $\sigma_{zz}$  for  $\zeta = 1.0$  clearly shows. Finally, if the fluid-substrate interaction exceeds that between a pair of fluid molecules (see plot for  $\zeta = 1.5$  in Fig. 9) the discontinuous change in  $\sigma_{zz}$  is replaced by a more continuous variation of the sorption

1  
2  
3 strain with pressure. However, comparing all three curves in Fig. 9 one concludes that the  
4 sequence of (weak) initial increase (beyond the pressure range of multilayer adsorption), a  
5 more or less abrupt decrease when the pore fills with liquid, and a subsequent increase of  
6 the sorption strain remains qualitatively unaffected provided the fluid-substrate interaction  
7 is sufficiently strong.  
8  
9

## 10 11 12 13 14 V. SUMMARY AND CONCLUSIONS

15  
16  
17 In this study we employ SGCMC simulations to study structure and phase behavior of a  
18 “simple” fluid confined between two atomically structured solid substrates. The substrate  
19 atoms are coupled thermally to one another and to the fluid molecules. In addition, each  
20 substrate atom is bound to its equilibrium lattice site by a harmonic “spring” where the  
21 binding parameter  $\kappa$  (i.e., the spring “stiffness”) controls the deformability (i.e., the “rigid-  
22 ity”) of the substrate. From a physical perspective thermal coupling between confined phases  
23 and the substrates causes the latter to “respond” to whatever changes there may be in the  
24 thermodynamic state of the former (and vice versa). Therefore, the confining substrates can  
25 no longer be treated as a static, inhomogeneous, external field, an approach taken by the  
26 overwhelming number of theoretical works on confined fluids to date.  
27  
28

29  
30 Thermal coupling of this sort complicates the statistical physical treatment of such model  
31 systems. This is because the substrate atoms may depart from their equilibrium sites on  
32 account of their thermal energy and as a result of the interactions constituting the thermal  
33 coupling to the confined fluid phase. More specifically, the configuration integral involves  
34 an integration over substrate-atom configurations in excess to the standard integration over  
35 configurations of the fluid phase.  
36  
37

38  
39 Our results indicate that for a sufficiently deformable substrate ( $\kappa = 30$ ) the effective  
40 pore width  $s_z^{\text{eff}}$  changes as the confined fluid undergoes a discontinuous phase transition  
41 from gas- to liquid-like phases. The size change of the pore can be expressed quantitatively  
42 in terms of a compressional strain which changes discontinuously at capillary condensation.  
43  
44 Under experimentally relevant conditions [45] the variation of the compressional strain with  
45 pressure turns out to be quite minute as far as the present subcritical thermodynamic states  
46 are concerned. Because the deformation of the substrate is in a sense determined by the  
47 magnitude of density fluctuations in the confined fluid (at a given rigidity of the substrate) we  
48  
49  
50  
51  
52  
53  
54  
55  
56  
57  
58  
59  
60

1  
2  
3 anticipate the effects reported here to be larger as one enters the near-critical regime of the  
4 confined phase. Work along these lines is currently under way [46]. The location of the phase  
5 transition is shifted to higher values of  $P/P_0 < 1$  compared with a fluid confined between  
6 rigid solid substrates indicating that the liquid phase is destabilized by pore deformation.  
7  
8  
9

10 This shift can be rationalized as follows [47]. Consider the limiting case  $\kappa = 0$  in which  
11 substrate atoms are no longer bound to their equilibrium lattice sites. Because the LJ poten-  
12 tial parameters  $\{\varepsilon, \sigma\}$  are the same for fluid-fluid, fluid-substrate, and substrate-substrate  
13 interactions our system degenerates into a bulk system in the limit  $\kappa = 0$ . Thus, in this limit  
14 one expects the condensation/evaporation of the fluid to occur at the bulk value  $P/P_0 = 1$ .  
15 on the other hand, for a rigid substrate as the other extreme case capillary condensation  
16 occurs at  $P/P_0 < 1$  where the shift of the phase transition relative to the bulk condensation  
17 is maximum. hence, for finite but nonzero values of  $\kappa$  one anticipates  $P/P_0$  at capillary  
18 condensation to be somewhere in between the values characteristic of the rigid substrate  
19 and the corresponding bulk system in agreement with plots in Figs. 3 and 4.  
20  
21  
22  
23  
24  
25  
26  
27

28 In this context it is important to realize that the case  $\kappa = 30$  complies with a realistic  
29 situation because this binding strength is still large enough so that the substrates are solid-  
30 like in character. This conclusion is drawn on the basis of the Lindemann criterion which  
31 assigns a specific value to the ratio  $\delta_L$  between the average root mean square displacement  
32 of solid atoms to the average nearest-neighbor distance at the melting point of the solid.  
33 According to work by Jin *et al.*  $\delta_L \approx 0.12$ – $0.13$  at the equilibrium melting temperature of  
34 a bulk crystal [43]. Moreover, as was demonstrated by Zhengming *et al.* in the one-phase  
35 region of a bulk crystal the surface layer of such a crystal exhibits less solid-like order than  
36 that characteristic of inner layers [44]. Thus, one anticipates a larger Lindemann ratio for  
37 the surface layer of a three-dimensional crystal. In this work we observe a value of  $\delta_L \approx 0.16$   
38 for the single-layer substrates which is still smaller than  $\delta_L \approx 0.2$  at which a bulk crystal  
39 becomes thermodynamically unstable [43]. Noticing that the substrates consist only of a  
40 single layer of atoms and in view of Refs. 43 and 44 we conclude that our substrates remain  
41 solid-like under the chosen thermodynamic conditions.  
42  
43  
44  
45  
46  
47  
48  
49  
50  
51  
52

53 Given that the conditions of this study seem sufficiently realistic what is the significance  
54 of thermal fluid-substrate coupling for parallel experiments? As we shall show in detail  
55 elsewhere [45] the strain measured for a nonpolar fluid adsorbed by mesoporous silica exhibits  
56 a pressure dependence in semi-quantitative agreement with the curve presented in Fig. 7 of  
57  
58  
59  
60

1  
2  
3 this work. Therefore, compared with the ideal case of rigid substrate surfaces one expects  
4 a shift of the location of the experimental phase transition similar to the one shown in  
5 Fig. 5(b) of this work. This shift, which should be of the order of a few percent, is large  
6 enough to be accessible experimentally *in principle*. However, in experiments the ideal case  
7 of rigid substrates can almost never be realized which makes a *direct* comparison with the  
8 present theoretical results rather challenging.  
9

10  
11 Nevertheless, the present study demonstrates a synergistic effect, that is the substrate  
12 responds to the thermodynamic state of the confined fluid which in turn affects the fluid's  
13 phase behavior. This synergistic effect is also expected to affect other types of phase transi-  
14 tions in nanoconfinement. For example, undercooled nanoconfined water does not freeze in  
15 the immediate vicinity of but only at larger distances from the pore walls, presumably on  
16 account of severe strains that prevent such vicinal water from forming solid-like structures  
17 [48]. These strains should be capable of deforming the pore walls similar to what is ob-  
18 served here. Another example are nanoconfined mesophases of anisometric molecules where  
19 molecular packing and orientation should exert strains on the pore walls. Implications from  
20 sorption strains on the phase behavior and vice versa might be expected particularly for  
21 fluids in very compliant nanoporous systems. A particular interesting case in this respect is  
22 the action of water in biological tissues, e.g., the movements of plants driven by changes in  
23 humidity [49].  
24  
25  
26  
27  
28  
29  
30  
31  
32  
33  
34  
35  
36  
37  
38

### 39 Acknowledgments

40  
41  
42 This work was supported by the Deutsche Forschungsgemeinschaft within the framework  
43 of the Sonderforschungsbereich 448 "Mesoskopisch strukturierte Verbundsysteme". More-  
44 over, we are indebted to S.H.L. Klapp (Technische Universität Berlin) and O. Paris (Max-  
45 Planck-Institut für Kolloid- und Grenzflächenforschung) for valuable discussions.  
46  
47  
48  
49  
50

---

51  
52  
53 [1] R. Evans and A.O. Parry, *J. Phys.: Condens. Matter* **2**, SA15 (1990).

54 [2] L.D. Gelb, K.E. Gubbins, R. Radhakrishnan, and M. Sliwinska-Bartkowiak, *Rep. Prog. Phys.*  
55 **62**, 1573 (1999).  
56  
57  
58  
59  
60

- 1  
2  
3 [3] M. Schoen and S.H.L. Klapp, *Nanoconfined fluids. Soft matter between two and three dimen-*  
4 *sions*, (Wiley-VCH, Hoboken, 2007).  
5  
6  
7 [4] W. Thomson (the later Lord Kelvin), *Phil. Mag.* **7**, 448 (1870).  
8  
9 [5] G.V. Burgess, D.H. Everett, and S. Nuttal, *Pure Appl. Chem.* **61**, 1845 (1989).  
10  
11 [6] A.P.Y. Wong and M.H.W. Chan, *Phys. Rev. Lett.* **65**, 2567 (1990).  
12  
13 [7] A. de Keizer, T. Michalski, and G.H. Findenegg, *Pure Appl. Chem.* **63**, 1495 (1991).  
14  
15 [8] A.P.Y. Wong, S.B. Kim, W.I. Goldberg, and M.H.W. Chan, *Phys. Rev. Lett.* **70**, 954 (1993).  
16  
17 [9] W.D. Machin, *Langmuir* **10**, 1235 (1994).  
18  
19 [10] M. Thommes and G.H. Findenegg, *Langmuir* **10**, 4270 (1994).  
20  
21 [11] D. Zhao, J. Feng, Q. Huo, N. Melosh, G.H. Frederickson, B.F. Chmelka, and G.D. Stucky,  
22 *Science* **279**, 548 (1998).  
23  
24 [12] D. Zhao, Q. Huo, J. Feng, B.F. Chmelka, and G.D. Stucky, *J. Am. Chem. Soc.* **120**, 6024  
25 (1998).  
26  
27 [13] T. Hoffmann, D. Wallacher, P. Huber, R. Birringer, K. Knorr, A. Schreiber and G.H. Find-  
28 enegg, *Phys. Rev. B* **72**, 064122 (2005).  
29  
30 [14] K. Binder, J. Horbach, A. Milchev, M. Müller, and R. Vink, *Comput. Phys. Commun.* **177**,  
31 140 (2007).  
32  
33 [15] M. Schoen, *Phys. Chem. Chem. Phys* **10**, 223 (2008).  
34  
35 [16] D.J. Diestler and M. Schoen, *J. Chem. Phys.* **104**, 6784 (1996).  
36  
37 [17] H. Namatsu, K. Kurihara, M. Nagase, K. Iwadate, and K. Murase, *Appl. Phys. Lett.* **66**, 2655  
38 (1995).  
39  
40 [18] P. Kowalczyk, A. Ciach, and A.V. Neimark, *Langmuir* **24**, 6603 (2008).  
41  
42 [19] E.A. Ustinov and D.D. Do, *Carbon* **44**, 2652 (2006).  
43  
44 [20] G.A. Zickler, S. Jähnert, W. Wagermeier, S.S. Funari, G.H. Findenegg, and O. Paris, *Phys.*  
45 *Rev. B* **73**, 184109 (2006).  
46  
47 [21] G.W. Scherer, *J. Am. Ceram. Soc.* **69**, 473 (1986).  
48  
49 [22] G. Dolino, D. Bellet, and C. Faivre, *Phys. Rev. B* **54**, 17919 (1996).  
50  
51 [23] T. Herman, J. Day, and J. Beamish, *Phys. Rev. B* **73**, 094127 (2006).  
52  
53 [24] K. Binder and P. Fratzl, in: *Materials Science and Technology, Vol. 5*, G. Kosterz (Ed.),  
54 (Wiley-VCH, Weinheim, 2001), p. 409.  
55  
56 [25] N.B. Wilding and M. Schoen, *Phys. Rev. E* **60**, 1081 (1999).  
57  
58  
59  
60

- 1  
2  
3 [26] J.P. Hansen and I.R. McDonald, *Theory of simple liquids*, (Academic Press, London, 1986).  
4  
5 [27] M. Schoen, *Ber. Bunsenges. Phys. Chem.* **100**, 8 (1996).  
6  
7 [28] R. Zwanzig, *J. Chem. Phys.* **22**, 1420 (1954).  
8  
9 [29] W.H. Press, B.P. Flannery, S.A. Teukolsky, and W.T. Vetterling, *Numerical recipes. The art*  
10 *of scientific computing (FORTRAN version)*, Chap. 4.  
11  
12 [30] J.E. Lane and T.H. Spurling, *Aust. J. Chem.* **29**, 2103 (1976).  
13  
14 [31] J. Mittal, J.R. Errington, and T.M. Truskett, *J. Chem. Phys.* **126**, 244708 (2007).  
15  
16 [32] I. Snook and W. van Megen, *J. Chem. Phys.* **70**, 3099 (1979).  
17  
18 [33] M. Schoen, J.H. Cushman, and D. J. Diestler, *J. Chem. Phys.* **87**, 1394 (1987).  
19  
20 [34] D.P. Cao, X.R. Zhang, Z.G. Shen, J.F. Chen, and J. Yun, *Phys. Rev. Lett.* **93**, 236105 (2004).  
21  
22 [35] A. Valencia and R. Lipowsky, *Langmuir* **20**, 1986 (2004).  
23  
24 [36] M. Schoen and S. Dietrich, *Phys. Rev. E* **56**, 499 (1997).  
25  
26 [37] A. O. Parry, C. Rascón, N. B. Wilding, R. Evans, *Phys. Rev. Lett.* **98**, 226101 (2007).  
27  
28 [38] H. Bohlen, A.O. Parry, E. Díaz-Herrera, and M. Schoen, *Eur. Phys. J. E* **25**, 103 (2008).  
29  
30 [39] A. Huerta, O. Pizio, and S. Sokolowski, *J. Chem. Phys.* **112**, 4286 (2000).  
31  
32 [40] S.T. Cui, P.T. Cummings, and H.D. Cochran, *Fluid Phase Equilib.* **183**, 381 (2001).  
33  
34 [41] T.M. Truskett, P.G. Debenedetti, and S. Torquato, *J. Chem. Phys.* **114**, 2401 (2001).  
35  
36 [42] A. Richter and T. Gruhn, *J. Chem. Phys.* **125**, 064908 (2006).  
37  
38 [43] Z.H. Jin, P. Gumbsch, K. Lu, and E. Ma, *Phys. Rev. Lett.* **87**, 055703 (2001).  
39  
40 [44] J. Zhengming, Y. Genqing, C. Zhaonian, L. Xianghuai, and Z. Shichang, *J. Phys.: Condens*  
41 *Matter* **6**, 1083 (1994).  
42  
43 [45] G. Günther, J. Prass, O. Paris, and M. Schoen, *Phys. Rev. Lett.*, in press.  
44  
45 [46] G. Günter and M. Schoen, in preparation.  
46  
47 [47] Private communication with O. Paris.  
48  
49 [48] A. Schreiber, I. Ketelsen, and G.H. Findenegg, *Phys. Chem. Chem. Phys.* **3**, 1185 (2001).  
50  
51 [49] R. Elbaum, L. Zaltzman, I. Burgert, and P. Fratzl, *Science* **316**, 884 (2007).  
52  
53  
54  
55  
56  
57  
58  
59  
60